Compression Strength of Composite Primary Structural Components

Semiannual Status Report

Eric R. Johnson
Principal Investigator

Performance Period: May 1, 1993 to October 31, 1993

NASA Grant NAG-1-537

Aerospace and Ocean Engineering Department
Virginia Polytechnic Institute and State University
Blacksburg, Virginia 24061-0203

October, 1993

Technical Monitor: Dr. James H. Starnes, Jr., Head
Aircraft Structures Branch
National Aeronautics and Space Administration
Langley Research Center
Hampton, Virginia 23681-0001

INTRODUCTION

Two projects are summarized in this report. The first project is entitled *Stiffener Crippling Initiated by Delamination*, and the second is entitled *Pressure Pillowing of an Orthogonally Stiffened Cylindrical Shell.*

RESEARCH ACCOMPLISHED

I. Stiffener Crippling Initiated by Delamination

Background and objective

Graphite-epoxy stiffeners tested in compression (Bonanni, Johnson, and Starnes, 1991) showed evidence of failure initiation in postbuckling by delamination at the free edges of the flanges. This mode of failure initiation occurred in *I*- and *J*-section specimens with flange width to thickness ratios in the range from ten to twenty. The analyses conducted in the Bonanni study modeled the stiffeners as a branched shell using the STAGS computer code. Since shell theories are based on plane stress and neglect through-the-thickness stress components, failure initiated by interlaminar stresses at the free edges of the flanges due to bending in postbuckling could not be studied with the STAGS model.

The objective of this project is to develop a computational model of the stiffener specimens that includes the capability to predict the interlaminar stress response at the flange free edge in postbuckling.

Presentation and Report

A presentation of this work was given at a professional meeting. The citation for this presentation is (speaker in boldface font)

- **Barlas, F. Aylin**, and Johnson, Eric R., "Interlaminar Stress Concentration in Postbuckled Open-Section Stiffeners," presented in session *Nonlinear Structural Mechanics – 1*, Joint SES/ASME/ASCE Meeting, University of Virginia, Charlottesville, Virginia, June 6-9, 1993

The following report was written and copies given to the technical monitor:

- Barlas, F. Aylin, and Johnson, Eric R., "Variable Complexity Modeling of Postbuckled Stiffeners for Delamination Initiation," Center for Composite Materials and Structures, Virginia Polytechnic Inst. and State Univ., Blacksburg, VA 24061, Rept. CCMS-93-11 and VPI-E-93-07, July 1993.

This report was the basis of Ms. Barlas's MS degree in Aerospace Engineering, which she successfully defended in June 1993. The abstract of this report follows:

Delamination at the free edge is analyzed as a mode of failure for uniaxial compression of

postbuckled structural components. Analyses are performed for I-section stiffeners and for a dropped -ply laminate, all of which failed due to free edge delamination in earlier studies. These specimens were made of AS4/3502 graphite-epoxy unidirectional tape. The nonlinear response of the specimens is modeled by a geometrically nonlinear finite element analysis. A variable-complexity modeling scheme is developed to economize computer resources for the nonlinear analysis. The three-dimensional stress field near the free edge is investigated by employing 20-node solid elements in that region. A dimensionless delamination index is calculated to investigate the severity of the interlaminar stress state. Numerical results correlated reasonably well with the experiments on the load-end shortening plots. The nodal lines and/or inflection points along the free edge in the postbucked configuration are found to be delamination critical sites. Both interlaminar shear stress tangent to the free edge and tensile interlaminar normal stress are significant at these critical locations and are likely to initiate delamination.

Interlaminar stress gradients

An important finding in the latest work involves the mesh refinement necessary to capture the stress gradients in the vicinity of the free edge of the postbuckled flange. The gradient in the interlaminar normal stress component in the direction of the normal to the edge is the fastest gradient, followed by the normal-direction gradient in the interlaminar shear stress component normal to the free edge, while the slowest gradients occur for the interlaminar shear stress component tangent to the free edge. Thus we found that the finite element mesh should be simultaneously refined in the direction normal to the free edge and through the thickness of flange in order to properly capture the stress gradient in the normal stress component. Mesh refinement did not significantly change the results for the interlaminar shear stress component tangent to the free edge. Early results obtained for specimens I2 and I10 were not converged to yield the results found in refined analysis in Sections 4.4.1 and 4.4.2 of the above cited report.

II. Pressure Pillowing of an Orthogonally Stiffened Cylindrical Shell

A conference paper was written on this project. The citation for it is

- Johnson, Eric R., and Rastogi, Naveen, "Interacting Loads in an Orthogonally Stiffened Composite Cylindrical Shell," Proceedings of Center for Adhesive and Sealant Science and Center for Composite Materials and Structures, Program Review, Donaldson Brown Hotel and Conference Center, Virginia Polytechnic Institute and State University, Blacksburg Virginia, October 3-5, 1993, pp. II.M.1 - II.M.15

The text of this conference paper is given at the end of this report.

Accumulative data for Grant NAG-1-537
November 1, 1984 to October 31, 1993

Publications Sponsored Under the Grant

Journal Papers

1. Bonanni, David L., Johnson, Eric R., and Starnes, James H., Jr., "Local Crippling of Thin-Walled Graphite-Epoxy Stiffeners", *AIAA Journal*, Vol. 29., No. 11, November 1991, pp. 1951-1959.

2. Curry, James H., Johnson, Eric R., and Starnes, James H., Jr., "Effect of Dropped Plies on the Strength of Graphite-Epoxy Laminates," *AIAA Journal*, Vol. 30, No.2, February 1992, pp. 449-456.

3. Dávila, Carlos G., and Johnson, Eric. R., "Analysis of Delamination Initiation in Postbuckled Dropped-Ply Laminates," *AIAA Journal*, Vol. 31, No. 4, April 1993, pp. 721 - 727.

Conference Papers

1. Lo, Patrick K-L, and Johnson Eric. R., "One-Dimensional Analysis of Filamentary Composite Beam Columns with Thin-Walled Open Sections," in ***Composites '86: Recent Advances in Japan and the United States***, K. Kawata, S. Umekawa & A. Kobayashi, Eds., Proceedings of the Third Japan-U.S. Conference on Composite Materials, Japan Society For Composite Materials, 1986, pp. 405-414. (Supported in part by NASA Grant NAG-1-343.)

2. Curry, James M., Johnson, Eric R., and Starnes, James H., Jr., "Effect of Dropped Plies on the Strength of Graphite-Epoxy Laminates," AIAA Paper No. 87-0874, in the proceedings of the *AIAA/ASME/ASCE/AHS 28th Structures, Structural Dynamics and Materials Conference*, Part 1, April 6-8, 1987, Monterey, California, pp. 737-747.

3. Bonanni, David L., Johnson, Eric., R., and Starnes, James H., Jr., "Local Crippling of Thin-Walled Graphite-Epoxy Stiffeners," AIAA Paper No. 88-2251, in the proceedings of the *AIAA/ASME/ASCE/AHS 29th Structures, Structural Dynamics and Materials Conference*, Part 1, April 18-20, 1988, Williamsburg, Virginia, pp. 313-323. (Supported in part by NASA Grant NAG-1-343.)

4. Johnson, E. R., and Bonanni, D. L., "Order 2p Derivatives from p-Differentiable Finite Element Solutions by a Spectral Method," in ***CAD/CAM, Robotics and Factories of the Future***, Vol. 1, Birendra Prasad, Ed., Springer-Verlag, Berlin, 1989, pp. 134-138.

5. Johnson, Eric R., and Dávila, Carlos G., "Compression Buckling of Thick Orthotropic Plates

with a Step Thickness Change," in the *Proceedings of the Twelfth Canadian Congress of Applied Mechanics*, Carleton University, Ottawa, Canada, M. A. Erki and J. Kirkhope, Eds., Vol. 1, 28 May - 2 June, 1989, pp. 140 & 141.

6. Haftka, Raphael T., and Johnson, Eric R., "Initial Postbuckling Response of an Unsymmetrically Laminated Rectangular Plate," in the Proceedings of the *Eighth DOD/NASA/FAA Conference on Fibrous Composites in Structural Design*, November 28-30, 1989, Norfolk, Virginia, NASA Conference Publication 3087, Part 2, 1990, pp. 609-623. (Supported in part by NASA Grant NAG-1-168.)

7. Dávila, Carlos G., and Johnson, Eric R., "Analysis for Delamination Initiation in Postbuckled Dropped-ply Laminates," AIAA Paper No. 92-2226, in the proceedings of *The 33rd AIAA/ ASME/ASCE/AHS/ASC Structures, Structural Dynamics and Materials Conference*, Part 1, April 13-15, 1992, Dallas Texas, pp. 29-39.

8. Johnson, Eric R., and Haftka, Raphael T., "Initial Postbuckling Response of Anisotropic Laminated Rectangular Plates," AIAA Paper No. 92-2284, in the proceedings of *The 33rd AIAA/ ASME/ASCE/AHS/ASC Structures, Structural Dynamics and Materials Conference*, Part 1, April 13-15, 1992, Dallas Texas, pp. 241-263. (Supported in part by NASA Grant NAG-1-168.)

9. Johnson, Eric R., and F. Aylin Barlas, "Interlaminar Stress Concentration in Postbuckled Open section Stiffeners," in *Mechanics of Composite Materials—Nonlinear Effects*, edited by M. W. Hyer, AMD-Vol. 159, American Society of Mechanical Engineers, New York, NY, 1993, pp. 19-28.

10. Johnson, Eric R., and Rastogi, Naveen, "Interacting Loads in an Orthogonally Stiffened Composite Cylindrical Shell," Proceedings of Center for Adhesive and Sealant Science and Center for Composite Materials and Structures, Program Review, Donaldson Brown Hotel and Conference Center, Virginia Polytechnic Institute and State University, Blacksburg Virginia, October 3-5, 1993, pp. II.M.1 - II.M.15.

Presentations

(Speaker indicated by boldface font.)

1. Lo, Patrick K-L, and **Johnson Eric. R.**, "One-Dimensional Analysis of Filamentary Composite Beam Columns with Thin-Walled Open Sections," in Session 10 Compression/Shear, The Third Japan-U.S. Conference on Composite Materials, June 23-25, 1986, Science University of Tokyo, Kagurazaka, Tokyo, Japan.

2. **Curry, James M.**, Johnson, Eric R., and Starnes, James H., Jr., "Effect of Dropped Plies on the Strength of Graphite-Epoxy Laminates," at the *AIAA/ASME/ASCE/AHS 28th Structures, Structural Dynamics and Materials Conference*, April 6-8, 1987, Monterey, California.

3. **Bonanni, David L.**, Johnson, Eric., R., and Starnes, James H., Jr., "Local Crippling of Thin-Walled Graphite-Epoxy Stiffeners," at the *AIAA/ASME/ASCE/AHS 29th Structures, Structural*

Dynamics and Materials Conference, April 18-20, 1988, Williamsburg, Virginia.

4. **Johnson, E. R.**, and Bonanni, D. L., "Order 2p Derivatives from p-Differentiable Finite Element Solutions by a Spectral Method," at the *3rd International Conference on CAD/CAM Robotics and Factories of the Future (CARS & FOF '88)*, Southfield, Michigan, August 14-17, 1988.

5. Johnson, Eric R., and **Dávila, Carlos G.**, "Compression Buckling of Thick Orthotropic Plates with a Step Thickness Change," Special Session: Mechanics of Laminated Structures, at the *Twelfth Canadian Congress of Applied Mechanics*, Carleton University, Ottawa, Canada, 28 May - 2 June, 1989.

6. Haftka, Raphael T., and **Johnson, Eric R.**, "Initial Postbuckling Response of an Unsymmetrically Laminated Rectangular Plate," Methodology and Design Session, at the *Eighth DOD/ NASA/FAA Conference on Fibrous Composites in Structural Design*, November 28-30, 1989, The Omni International Hotel, Norfolk, Virginia.

7. **Foster, John L.**, and Johnson, Eric R., "Computation of Interlaminar Stresses From Finite Element Solutions to Plate Theories," Session 35: Work in Progress II, at *The 32nd AIAA/ ASME/ASCE/AHS/ASC Structures, Structural Dynamics and Materials Conference*, April 8-10, 1991, Hyatt Regency Baltimore, Baltimore, Maryland.

8. **Dávila, Carlos G.**, and Johnson, Eric R., "Analysis for Delamination Initiation in Postbuckled Dropped-ply Laminates," Session 5: Damage Tolerance of Composites, at *The 33rd AIAA/ ASME/ASCE/AHS/ASC Structures, Structural Dynamics and Materials Conference*, April 13-15, 1992, Grand Kempinski Hotel, Dallas, Texas.

9. **Johnson, Eric R.**, and Haftka, Raphael T., "Initial Postbuckling Response of Anisotropic Laminated Rectangular Plates," Session 14: Buckling/Postbuckling of Plates and Stiffened Panels, at *The 33rd AIAA/ASME/ASCE/AHS/ASC Structures, Structural Dynamics and Materials Conference*, April 13-15, 1992, Grand Kempinski Hotel, Dallas, Texas.

10. **Johnson, Eric R.**, and Rastogi, Naveen, "Interacting Loads in an Orthogonally Stiffened Composite Cylindrical Shell," presented in Session 25 — Work-in-Progress 1, at *The 34th AIAA/ASME/ASCE/AHS/ASC Structures, Structural Dynamics and Materials Conference*, April 19-21, 1993, Hyatt Regency, La Jolla, California.

11. **Barlas, F. Aylin**, and Johnson, Eric R., "Interlaminar Stress Concentration in Postbuckled Open-Section Stiffeners," presented in session *Nonlinear Structural Mechanics – 1*, Joint SES/ASME/ASCE Meeting, University of Virginia, Charlottesville, Virginia, June 6-9, 1993.

12. Johnson, Eric R., and **Rastogi, Naveen**, "Interacting Loads in an Orthogonally Stiffened Composite Cylindrical Shell," in Composite Session 3: Composite Structures – Analysis and Rehabilitation, Center for Adhesive and Sealant Science and Center for Composite Materials and Structures, Program Review, Donaldson Brown Hotel and Conference Center, Virginia Polytechnic Institute and State University, Blacksburg, Virginia, October 3-5, 1993.

Reports

1. Curry, J. M., Johnson, E. R., and Starnes, J. H., Jr., "Effect of Ply Drop-Offs on the Strength of Graphite-Epoxy Laminates," Center for Composite Materials and Structures, Virginia Polytechnic Inst. and State Univ., Blacksburg, VA 24061, Rept. CCMS-86-07 and VPI-E-86-27, December 1986.

2. Bonanni, D. L., Johnson, E. R., and Starnes, J. H., Jr., "Local Buckling and Crippling of Composite Stiffener Sections," Center for Composite Materials and Structures, Virginia Polytechnic Inst. and State Univ., Blacksburg, VA 24061, Rept. CCMS-88-08 and VPI-E-88-15, June 1988. (Supported in part by NASA Grant NAG-1-343.)

3. Foster, J. L., and Johnson, E. R., "Computation of Interlaminar Stresses From Finite Element Solutions to Plate Theory," Center for Composite Materials and Structures, Virginia Polytechnic Inst. and State Univ., Blacksburg, VA 24061, Rept. CCMS-91-10 and VPI-E-91-10, June 1991.

4. Dávila, C. G., and Johnson, E. R., "Delamination Initiation in Postbuckled Dropped-ply Laminates," Center for Composite Materials and Structures, Virginia Polytechnic Inst. and State Univ., Blacksburg, VA 24061, Rept. CCMS-91-24 and VPI-E-91-23, December 1991.

5. Dávila, Carlos G. and Johnson, Eric R., "The Computational Structural Mechanics Testbed: User's Manual for Transition Elements in Processor ES16," Aerospace and Ocean Engineering, Virginia Polytechnic Institute and State University, Blacksburg, Virginia 24061-0203, February 1992, (draft).

6. Barlas, F. Aylin, and Johnson, Eric R., "Variable Complexity Modeling of Postbuckled Stiffeners for Delamination Initiation," Center for Composite Materials and Structures, Virginia Polytechnic Inst. and State Univ., Blacksburg, VA 24061, Rept. CCMS-93-11 and VPI-E-93-07, July 1993.

Students Earning Degrees and Funded Under the Grant

1. James M. Curry, Master of Science in Aerospace Engineering, May 1986.
   Thesis Title: Effect of Ply Drop-Offs on the Strength of Graphite-Epoxy Laminates
   Initial Employer: Rohr Industries, Inc., Chula Vista CA

2. David L. Bonanni, Master of Science in Aerospace Engineering, April 1988.
   Thesis Title: Local Crippling of Composite Stiffener Sections
   Initial Employer: David Taylor Research Center, Bethesda MD
   (Supported in part by NASA Grant NAG-1-343.)

3. John L. Foster, Master of Science in Aerospace Engineering, April 1991.
   Thesis Title: Computation of Interlaminar Stresses from Finite Element Solutions to Plate Theory
   Initial Employer: McDonnell Douglas Space Systems Co., Huntington Beach CA.

4. Carlos G. Dávila, Doctor of Philosophy in Aerospace Engineering, November 1991
   Dissertation Title: Delamination Initiation in Postbuckled Dropped-Ply Laminates
   Initial Position: National Research Council Resident Research Associate,
   NASA Langley Research Center, Hampton VA

5. F. Aylin Barlas, Master of Science in Aerospace Engineering, June 1993
   Thesis Title: Variable Complexity Modeling of Postbuckled Stiffeners for Delamination Initiation

Interacting loads in an orthogonally stiffened composite cylindrical shell

Eric R. Johnson[1] and Naveen Rastogi[2]

Aerospace and Ocean Engineering Department
Virginia Polytechnic Institute and State University
Blacksburg, VA 24061-0203

Abstract

The distributions of the interacting loads between orthogonal stiffeners and the shell wall are computed for a long circular cylindrical shell subjected to internal pressure. Identical stringers are equally spaced around the circumference, and identical frames, or rings, are equally spaced along the length. Both the stringers and frames are on the inside of the shell wall. Closed-end pressure vessel effects are included. A comparison is made between the linear elastic response and geometrically nonlinear elastic response. The example problem has dimensions of the fuselage of a typical transport aircraft, and has a composite material shell wall and symmetric stiffeners.

Introduction

The cabin pressure in a transport aircraft causes about a 10 psi pressure differential across the skin. An unstiffened, or monocoque, fuselage would carry this internal pressure load as a shell in membrane response, like a pressure vessel. However, internal longitudinal and transverse stiffeners are necessary to carry maneuver loads, etc. The presence of these internal stiffeners prevents the fuselage skin from expanding as a membrane, and the skin bulges, or "pillows", between the stiffeners under the action of the internal pressure. Where the skin is restrained against its expansion as a membrane along the stiffeners, a bending boundary layer is formed. Also, at the stiffener intersection a local concentration of the interacting loads between the stiffeners and the skin occurs. Hence, the objectives of this paper are 1) to analyze the concentration of the interacting loads at the stiffener intersection, and 2) to study the pillowing of the skin, for both a linear response and a geometrically nonlinear response of a fuselage subjected to internal pressure.

Mathematical model

An idealized mathematical model is assumed for the semi-monocoque fuselage to study the generic characteristics of the response in the vicinity of the stiffener intersection. The model is of a very long circular cylindrical shell internally stiffened by identical stringers equally spaced around the circumference, and identical frames, or rings, equally spaced along the length. In general, the spacing of the stringers is not the same as the rings. The structure is periodic both longitudinally and circumferentially, and the loading is spatially uniform. Consequently, a structural repeating unit can be defined whose deformation determines the deformation of the entire structure. The repeating unit consists of a portion of the shell wall centered over portions of the stringer and ring as shown in Fig. 1. The radius of the middle surface of the undeformed cylinder is denoted by R, and thickness of the cylindrical shell is denoted by t. Axial coordinate x and the circumferential angle θ are lines of curvature on the middle surface, and the thickness coordinate is denoted by ζ, with $-t/2 \le \zeta \le t/2$. The origin of the surface coordinates is centered over the stiffener intersection so that $-l \le x \le l$ and $-\Theta \le \theta \le \Theta$, where $2l$ is the axial length, and $2R\Theta$ is the circumferential arc length, of the repeating unit.

The stiffeners are modeled as mathematically one-dimensional structural elements, such that the actions transmitted by the stiffeners to the inside surface of the shell wall are represented by distributed line loads as shown in Fig. 2. In this paper it is assumed that the stringer is symmetric about the x-ζ plane through its centroidal axis, and the ring is symmetric about the θ–ζ plane through its circular reference axis. On the basis of the symmetry about the x– and θ–axes for the unit, only the interacting load components tangent and normal to the stiffeners are included in the analysis. The interacting load intensities per unit undeformed length along the contact lines are denoted by $\lambda_{xs}(x)$ for the

1. Associate Professor
2. Graduate Research Assistant

component tangent to the stringer, $\lambda_{\zeta s}(x)$ for the component normal to the stringer, $\lambda_{\theta r}(\theta)$ for the component tangent to the ring, and by $\lambda_{\zeta r}(\theta)$ for the component normal to the ring. The positive directions for these interacting loads acting on the shell are shown in Fig. 2. The purpose of the analysis is to determine these distributed line loads.

An enclosed volume to contain the pressurized medium is modeled by assuming diaphragms to extend from the edges of the repeating unit to the axis of revolution of the cylinder. The diaphragms do not resist the deformation of the repeating unit, but act to transmit loads normal to the edges of the repeating unit due to the internal pressure.

For both the linear and nonlinear response of the repeating unit to internal pressure, we use the Ritz method and the principle of virtual work augmented by Lagrange multipliers to enforce kinematic constraints between the structural components of the repeating unit. The Lagrange multipliers represent the interacting line loads between the stiffeners and the shell. Displacements are separately assumed for the shell, stringer, and ring.

Displacement and Lagrange multiplier approximations

The periodic portions of the displacements are represented by truncated Fourier Series, and the nonperiodic portions of the displacements due to axial stretching are represented by simple terms in x. For the shell, the displacements of the middle surface are

$$u(x,\theta) = \sum_{m=1}^{M}\sum_{n=0}^{N} u_{mn}\sin(\alpha_m x)\cos(\beta_n\theta) + \frac{q_0 x}{2l}, \tag{1}$$

$$v(x,\theta) = \sum_{m=0}^{M}\sum_{n=1}^{N} v_{mn}\cos(\alpha_m x)\sin(\beta_n\theta), \tag{2}$$

$$w(x,\theta) = \sum_{m=0}^{M}\sum_{n=0}^{N} w_{mn}\cos(\alpha_m x)\cos(\beta_n\theta), \tag{3}$$

in which $\alpha_m = (m\pi)/l$ and $\beta_n = (n\pi)/\Theta$ where m and n are non-negative integers. The displacements of the centroidal axis of the stringer are

$$u_s(x) = \sum_{m=1}^{M} u_{sm}\sin(\alpha_m x) + \frac{q_1 x}{2l} \qquad w_s(x) = \sum_{m=0}^{M} w_{sm}\cos(\alpha_m x) \tag{4}$$

Parameters q_0 in the axial displacement of the shell and q_1 in the axial displacement of the stringer represent elongations of each respective element caused by either an axial mechanical load or due to closed-end pressure vessel effects. The displacements of the reference circle of the ring are

$$v_r(\theta) = \sum_{n=1}^{N} v_{rn}\sin(\beta_n\theta) \qquad w_r(\theta) = \sum_{n=0}^{N} w_{rn}\cos(\beta_n\theta) \tag{5}$$

The distributions of the Lagrange multipliers, or interacting loads, are taken as

$$\lambda_{xs} = \sum_{m=1}^{M} \lambda_{xsm}\sin(\alpha_m x) \qquad \lambda_{\zeta s} = \sum_{m=1}^{M} \lambda_{\zeta sm}\cos(\alpha_m x), \tag{6}$$

$$\lambda_{\theta r} = \sum_{n=1}^{N} \lambda_{\theta rn}\sin(\beta_n\theta) \qquad \lambda_{\zeta r} = \sum_{n=0}^{N} \lambda_{\zeta rn}\cos(\beta_n\theta). \tag{7}$$

Note that in the stringer interacting normal load, the term $\lambda_{\zeta s0}$, which represents a uniformly distributed load, is omitted. Since the stringer as modeled by this analysis is not restrained from rigid body motion in the normal direction the resultant normal load on the stringer must vanish; i.e.,

$$\int_{-l}^{l} \lambda_{\zeta_s}(x)\, dx = 0, \tag{8}$$

and this condition requires $\lambda_{\zeta s0}$ to vanish.

Virtual work

Shell

The generalized strain vector for the shell is

$$\vec{\varepsilon}_{shell} = [\varepsilon_{xx}, \varepsilon_{\theta\theta}, \gamma_{x\theta}, \kappa_{xx}, \kappa_{\theta\theta}, \kappa_{x\theta}]^T \tag{9}$$

Assuming the strains are small and rotations are moderately small, the membrane strain-displacement relations are[1]

$$\varepsilon_{xx} = \frac{\partial u}{\partial x} + \frac{1}{2}\phi_x^2 + \frac{1}{2}\phi^2 \qquad \varepsilon_{\theta\theta} = \frac{1}{R}\left(\frac{\partial v}{\partial \theta} + w\right) + \frac{1}{2}\phi_\theta^2 - \frac{1}{2}\phi^2 \qquad \gamma_{x\theta} = \frac{1}{R}\frac{\partial u}{\partial \theta} + \frac{\partial v}{\partial x} + \phi_x\phi_\theta, \tag{10}$$

in which ϕ_x is the rotation of the normal around the θ-curve, ϕ_θ is the rotation of the normal around the x-curve, and ϕ is the rotation around the normal. The rotations are given by

$$\phi_x = -\frac{\partial w}{\partial x} \qquad \phi_\theta = -\frac{1}{R}\frac{\partial w}{\partial \theta} + \frac{v}{R} \qquad \phi = \frac{1}{2}\left[\frac{\partial v}{\partial x} - \frac{1}{R}\frac{\partial u}{\partial \theta}\right] \tag{11}$$

The change in the normal curvature components in terms of the rotations are

$$\kappa_{xx} = \frac{\partial \phi_x}{\partial x} \qquad \kappa_{\theta\theta} = \frac{1}{R}\frac{\partial \phi_\theta}{\partial \theta} \qquad \kappa_{x\theta} = \frac{\partial \phi_\theta}{\partial x} + \frac{1}{R}\frac{\partial \phi_x}{\partial \theta} + \frac{1}{R}\phi. \tag{12}$$

The Donnell-Mushtari-Vlasov (DMV) approximation, or quasi-shallow shell theory, is obtained by neglecting the rotation about the normal in the strains of Eqs. (10) and (12), and the shaded term in rotation ϕ_θ of Eq. (11). We assume that the contribution of the rotation about the normal to the strains is negligible for the shell, but do not assume the DMV approximation initially.

Define the generalized stress vector in terms of the stress resultants and couples of Sander's theory[1,2] by

$$\vec{\sigma}_{shell} = [N_{xx}, N_{\theta\theta}, N_{x\theta}, M_{xx}, M_{\theta\theta}, M_{x\theta}]^T, \tag{13}$$

such that the internal virtual work is

$$\delta W_{shell}^{int} = \iint_S \delta\vec{\varepsilon}_{shell}^{\,T}\ \vec{\sigma}_{shell}\ dS, \tag{14}$$

where S denotes the area of the middle surface and $dS = dx\, Rd\theta$. For a laminated composite material shell wall, Hooke's law is

$$\vec{\sigma}_{shell} = H\vec{\varepsilon}_{shell} \qquad H = \begin{bmatrix} A & B \\ B^T & D \end{bmatrix}. \tag{15}$$

in which the 3×3 submatrices A, B, and D are given by classical lamination theory[3].

The statement of virtual work is

$$\delta W^{int}_{shell} = \delta W^{ext}_{p} + \int_{-l}^{l} \{\lambda_{xs}(x)\,\delta\left[u(x,0) - \frac{t}{2}\phi_x(x,0)\right] + \lambda_{\zeta_s}(x)\,\delta w(x,0)\}\ dx$$
$$+ \int_{-\Theta}^{\Theta} \{\lambda_{\theta r}(\theta)\,\delta\left[v(0,\theta) - \frac{t}{2}\phi_\theta(0,\theta)\right] + \lambda_{\zeta_r}(\theta)\,\delta w(0,\theta)\}\ (R - \frac{t}{2})\,d\theta \tag{16}$$

for every admissible variation in the shell displacements. For an enclosed volume, the work done by a constant hydrostatic pressure is conservative. (Note that the pressure remains normal to the deformed surface.) In terms of shell displacements, the work functional for the constant hydrostatic pressure p is

$$W^{ext}_{p} = p\iint_{S}\left((1+u_x)\,(w + \frac{1}{2R}(w^2+v^2)) + v_y w + \frac{1}{3}det\begin{bmatrix} u & v & w \\ u_x & v_x & w_x \\ u_y & v_y & w_y \end{bmatrix}\right) dS$$
$$+ \left(pR^2\Theta + \frac{p}{6}\int_{-\Theta}^{\Theta} (v_y w - v w_y)\,|_{x=l}\ R\,d\theta - Q\right) q_0 \tag{17}$$

in which $y = R\theta$, and we denoted partial derivatives of the displacements by a subscript. The second term in Eq. (17) corresponds to the work of the pressure on diaphragms at $x = \pm l$ less the portion Q of this axial load that is carried by the stringer. The axial force Q is an additional Lagrange multiplier that accounts for axial load sharing between the stringer and shell.

Stringer

The virtual work statement for the stringer is

$$\delta\int_{-l}^{l} (N_{xs}\delta\varepsilon_{xs} + M_{xs}\delta\kappa_{xs})\,dx = -\int_{-l}^{l} \{\lambda_{xs}(x)\,\delta[u_s(x) - e_s w'_s(x)] + \lambda_{\zeta_s}(x)\,\delta w_s(x)\}\,dx + Qq_1 \tag{18}$$

in which N_{xs} is the axial force in the stringer, M_{xs} is the bending moment, ε_{xs} is the extensional normal strain of the centroidal line, κ_{xs} is the change in curvature of the centroidal line, e_s is the radial distance from the stringer centroid to the contact line along the shell inside surface, and the prime superscript denotes ordinary derivative with respect to x. The strain-displacement relations and Hooke's law for the stringer are

$$\varepsilon_{xs} = u'_s + \frac{1}{2}(w'_s)^2 \qquad \kappa_{xs} = -w''_s, \tag{19}$$

$$N_{xs} = (EA)_s\varepsilon_{xs} \qquad M_{xs} = (EI)_s\kappa_{xs} \tag{20}$$

Ring

The virtual work statement for the ring is

$$\int_{-\Theta}^{\Theta} (N_{\theta r}\delta\varepsilon_{\theta r} + M_{\theta r}\delta\kappa_{\theta r})\,R_0\ d\theta = -\int_{-\Theta}^{\Theta} \{\lambda_{\theta r}\delta[v_r + e_r\phi_r] + \lambda_{\zeta_r}\delta w_r\}\left(1 + \frac{e_r}{R_0}\right)R_0 d\theta, \tag{21}$$

in which $N_{\theta r}$ is the circumferential force, $M_{\theta r}$ is the bending moment, $\varepsilon_{\theta r}$ is the circumferential normal strain of the reference arc, $\kappa_{\theta r}$ is the change in curvature of the reference arc, and the radius of the contact circle between the ring and shell is $R_0 + e_r = R - t/2$. The rotation, strain-displacement relations, and Hooke's law for the ring are

$$\phi_r = \frac{1}{R_0}(v_r - \dot{w}_r) \qquad \varepsilon_{\theta r} = \frac{1}{R_0}(\dot{v}_r + w_r) + \frac{1}{2}\phi_r^2 \qquad \kappa_{\theta r} = \frac{1}{R_0}\dot{\phi}_r, \tag{22}$$

$$N_{\theta r} = (EA)_r \varepsilon_{\theta r} \qquad M_{\theta r} = (EI)_r \kappa_{\theta r} \tag{23}$$

in which the over-dot denotes and an ordinary derivative with respect to θ.

Displacement continuity

Displacement continuity constraints along the contact lines between the stiffeners and the inside surface of the shell are

$$g_{xs}(x) = u(x,0) - \frac{t}{2}\phi_x(x,0) - \left[u_s(x) - e_s\frac{dw_s}{dx}\right] = 0 \tag{24}$$

$$g_{\zeta s}(x) = w(x,0) - w_s(x) = 0 \tag{25}$$

$$g_{\theta r}(\theta) = v(0,\theta) - \frac{t}{2}\phi_\theta(0,\theta) - [v_r(\theta) + e_r\phi_r(\theta)] = 0 \tag{26}$$

$$g_{\zeta r}(\theta) = w(0,\theta) - w_r(\theta) = 0 \tag{27}$$

The variational form for these constraints are

$$\int_{-l}^{l} (\delta\lambda_{xs} g_{xs} + \delta\lambda_{\zeta s} g_{\zeta s})\, dx = 0 \qquad \int_{-\Theta}^{\Theta} (\delta\lambda_{\theta r} g_{\theta r} + \delta\lambda_{\zeta r} g_{\zeta r})\,(R_0 + e_r)\, d\theta = 0. \tag{28}$$

The constraint that the elongation of the shell at θ = 0 and the stringer are the same is

$$\delta Q\,[q_1 - q_0] = 0. \tag{29}$$

Satisfying the variational form of the constraints, Eqs. (28) and (29), is not sufficient, in general, to satisfying the constraints pointwise, Eqs. (24-27). Since the trigonometric Fourier Series functions are linearly independent, and Eq. (29) separately satisfies the polynomial terms in the axial displacements, the satisfaction of the variational constraints in this analysis does lead to satisfying the constraints pointwise.

Discrete equations and their solution

The discrete displacement vector for the shell is the *(3MN+2M+2N +2)* × *1* vector

$$\hat{u}_{shell} = [\hat{u}_0^T, \hat{u}_1^T, \ldots, \hat{u}_M^T]^T \tag{30}$$

in which the subvectors are

$$\hat{u}_0 = [q_0, w_{00}, v_{01}, w_{01}, \ldots, v_{0N}, w_{0N}]^T$$
$$\hat{u}_m = [u_{m0}, w_{m0}, u_{m1}, v_{m1}, w_{m1}, \ldots u_{mN}, v_{mN}, w_{mN}]^T \qquad m = 1, \ldots, M \tag{31}$$

The *(2M + 1)* × *1* discrete displacement vector for the stringer and the *(2N + 1)* ×*1* vector for the ring are

$$\hat{u}_{str} = [q_1, u_{s1}, w_{s1}, \ldots, u_{sM}, w_{sM}]^T \qquad \hat{u}_r = [w_{r0}, v_{r1}, w_{r1}, \ldots, v_{rN}, w_{rN}]^T, \tag{32}$$

in which the term w_{s0} for the stringer has been omitted since it does not deform the stringer and its conjugate resultant in Eq. (8) is equal to zero. This uniform normal displacement component is determined from the condition that the rigid body displacement of the stringer is the uniform portion of the normal displacement component of the shell at θ = 0; i.e.,

$$\sum_{n=0}^{N} w_{0n} = w_{s0}. \tag{33}$$

The discrete vectors of the Lagrange multipliers are

$$\hat{\lambda}_{str} = [\lambda_{xs1}, \lambda_{\zeta s1}, \ldots, \lambda_{xsM}, \lambda_{\zeta sM}]^T \qquad \hat{\lambda}_r = [\lambda_{\zeta r0}, \lambda_{\theta r1}, \lambda_{\zeta r1}, \ldots, \lambda_{\theta rN}, \lambda_{\zeta rN}]^T. \tag{34}$$

For the nonlinear problem an iterative solution procedure is required. At a fixed value of the pressure p, a sequence of displacements is defined by adding an increment to the previous member of the sequence to determine the next member in the sequence. For a good initial displacement estimate, the sequence converges to the displacement solution of the nonlinear problem. The initial estimate used here is the converged solution at the last pressure load step. The update procedure to determine the increment is based on the modified Newton-Raphson method. To obtain the equations for the Newton-Raphson method, we first derived the virtual work functionals for the shell, stringer, and ring, based on replacing the displacement components by a generic member in their sequence plus an increment. Then the functionals are linearized in the increments. Second, the approximations in Eqs. (1) to (5) are substituted into the incremented virtual work functionals for the displacements, and similar forms are substituted for their increments. Integration over space is performed after substitution of Eqs. (6) and (7) for the Lagrange multipliers, and after substitution for the variational displacements and the variational Lagrange multipliers. (The variational displacements and the variational Lagrange multipliers use the same space of functions as their unvaried forms given in Eqs. (1-7).) This process results in a $3MN + 6M + 6N + 6$ system of equations governing the increment in the displacements (indicated by a Δ preceding the displacement subvector symbol) and the Lagrange multipliers. These equations are

$$\begin{bmatrix} K_{11}(\hat{u}_{shell}) - pL(\hat{u}_{shell}) & 0 & 0 & B_{11} & B_{12} & B_{13} \\ 0 & K_{22}(\hat{u}_{str}) & 0 & B_{21} & 0 & B_{23} \\ 0 & 0 & K_{33}(\hat{u}_r) & 0 & B_{32} & 0 \\ B_{11}^T & B_{21}^T & 0 & 0 & 0 & 0 \\ B_{12}^T & 0 & B_{32}^T & 0 & 0 & 0 \\ B_{13}^T & B_{23}^T & 0 & 0 & 0 & 0 \end{bmatrix} \begin{bmatrix} \Delta\hat{u}_{shell} \\ \Delta\hat{u}_{str} \\ \Delta\hat{u}_r \\ \hat{\lambda}_{str} \\ \hat{\lambda}_r \\ Q \end{bmatrix} = \begin{bmatrix} \hat{R}_{shell}(\hat{u}_{shell};\ p) \\ \hat{R}_{str}(\hat{u}_{str}) \\ \hat{R}_r(\hat{u}_r) \\ 0 \\ 0 \\ 0 \end{bmatrix} \tag{35}$$

in which K_{11}, K_{22}, and K_{33} are the tangent stiffness matrices for the shell, stringer, and ring, respectively, that are functions of the displacements. The matrix L results from the nonlinear portion of the external work functional for the hydrostatic pressure, Eq.(17). In the modified Newton-Raphson method these matrices K_{11}, K_{22}, K_{33}, and L are only computed for the initial displacement in the sequence, and are not updated for each new member in the sequence. The submatrices B_{ij}, $i,j = 1, 2, 3$, in Eq. (34) are determined from the external virtual work terms involving the Lagrange multipliers, and the constraint Eqs. (28) and (29). These B_{ij} submatrices are not functions of the displacements. The vector on the right-hand-side of Eq. (35) is the residual force vector, which vanishes at equilibrium for the repeating unit. The constraint equations correspond to the last three rows of the partitioned matrix in Eq. (35), and as shown in Eq. (35) these constraints are applied to the increments in the displacements. If the initial estimate of the displacement satisfies these constraint equations and the increments satisfy these same equations, then the final displacement in the sequence will satisfy these same equations. Equation (35) is solved first for the increments in the displacements in terms of the Lagrange multipliers, then this solution is substituted into the constraint equations to determine the Lagrange multipliers. Thus, the total solution is obtained.

Numerical example

Data for the example are $2l = 20$ in., $R = 117.5$ in., $2R\Theta = 5.8$ in., $t = 0.075$ in., $R_0 = 113.72$ in., $e_s = 1.10$ in., $e_r = 3.78$ in., $(EA)_r = 0.592 \times 10^7$ lb., $(EI)_r = 0.269 \times 10^8$ lb-in^2, $(EA)_s = 0.404 \times 10^7$ lb., $(EI)_s = 0.142 \times 10^8$ lb-in^2, and with the shell wall stiffness matrices given by

$$A = \begin{bmatrix} 0.664 & 0.221 & 0 \\ 0.221 & 0.577 & 0 \\ 0 & 0 & 0.221 \end{bmatrix} \times 10^6 \text{ lb/in} \qquad B = 0 \qquad D = \begin{bmatrix} 262 & 159 & 4.33 \\ 159 & 210 & 4.33 \\ 4.33 & 4.33 & 159 \end{bmatrix} \text{ lb-in}.$$

This data was originally used in an example by Wang and Hsu[4], and the dimensional data is representative of a large transport fuselage. All the results presented for this example are for an internal pressure $p = 10$ psi. The Fourier Series were truncated at $M = N = 16$, unless otherwise indicated. Since $2\Theta = 2.83°$, the shell in this example is shallow and the DMV shell theory should be adequate. We found that the numerical results using Sanders theory with the rotation about the normal neglected and the numerical results using DMV theory were essentially the same.

Results and discussion

Pillowing

Circumferential distributions of the normal displacement w for the shell are shown in Fig. 3 for the linear analysis and in Fig. 4 for the nonlinear analysis. Axial distributions of w are shown in Fig. 5 for the linear analysis and in Fig. 6 for the nonlinear analysis. For reference, the normal displacement for the unstiffened shell, or membrane response, is $w = 0.2287$ inches for the linear analysis, and $w = 0.2290$ inches for the nonlinear analysis. The presence of the stiffeners reduces the normal displacements from these membrane values as is shown in the figures. The w-distributions shown for the linear analysis compare very well with those presented by Wang and Hsu[4]. (Wang and Hsu's results are limited to linear analysis.). The pillowing effect is much more pronounced for the linear analysis (Figs. 3 and 5) than for the nonlinear analysis (Figs. 4 and 6). The largest normal displacement occurs midway between the stiffeners, and this value for the linear analysis is 0.1796 inches while it is 0.1541 inches when geometric nonlinearity is included. The minimum normal displacement occurs at the stiffener intersection (not shown in the figures), and its value is 0.1392 inches in the linear analysis and 0.1490 inches in the nonlinear analysis. Normal displacements along the stiffeners vary only slightly from their values at the intersection for both analyses. Thus, including geometric nonlinearity in the analysis increases the minimum value of the normal displacement of the shell and decreases its maximum value, which is an indication that pillowing is reduced in the nonlinear response.

The circumferential and axial normal strain distributions on the inner and outer surfaces of the shell also show the reduced pillowing effect in the nonlinear analysis. See Figs. 7-10. The circumferential bending strain (difference in $\varepsilon_{\theta\theta}$ between the inner and outer surfaces) is maximum at the stringer midway between the rings (Figs. 7 and 8), and the axial bending strain is maximum at the ring midway between the stringers (Figs. 9 and 10). These maximum bending strains are substantially reduced in the geometrically nonlinear response relative to the linear response. The values of the ε_{xx} and $\varepsilon_{\theta\theta}$ strains from the linear analysis (Figs. 7 and 9) compare very well to those presented by Wang and Hsu, except in one respect. The exception is that the circumferential distribution of the axial strain ε_{xx} at $x = -l$ (Fig. 9) does not exhibit a decrease in value as the stringer is approached. Wang and Hsu's results, however, show ε_{xx} decreasing to nearly zero as the stringer is approached along the circumference. We attempted several changes to the shell displacement approximations, and even programmed Wang and Hsu's solution, but could not get any of these attempts to give a solution showing a decrease in the axial normal strain at the stringer.

Interacting load distributions

The distributions of the interacting loads between the ring and shell are shown in Figs. 11 and 12. The distribution of the circumferential component (Fig. 11) is antisymmetric about the origin, and has reduced magnitudes due to the geometrically nonlinear effect. As shown in Fig. 12, the normal component of the interacting load is an extremum at the origin, exhibiting a severe gradient there. The negative value of λ_{ζ_r} at the origin indicates that the action of the ring is to pull the shell radially inward against the action of the pressure to expand the shell outward. The peak normal load intensity is reduced from -1,674 lb/in in the linear analysis to -1,045 lb/in in the nonlinear analysis.

The distributions of the interacting loads between the stringer and the shell are shown in Figs. 13 and 14. The distribution of the tangential component is antisymmetric about the origin and has reduced peak magnitudes due to the geometrically nonlinear effect as shown in Fig. 13. The normal component λ_{ζ_s} is maximum at the origin and has a steep gradient there as shown in Fig. 14. The maximum value of normal component is reduced from 484.7 lb/in in the

linear analysis to 320.3 lb/in the nonlinear analysis. Note that the resultant of this normal component vanishes as a result of Eq. (8).

Stiffener actions

The distribution of the force and moment resultants in the stiffeners are shown in Figs. 15 and 16. In the linear analysis the total axial load due to the 10 psi pressure is 3,407.5 lbs (the $pR^2\Theta$ term multiplying q_0 in Eq. (17)), and the portion of this load carried by the stringer is 820.1 lbs, or about 24% of the total axial load, according to the value of N_{xs} at $x = \pm l$ shown in Fig. 15. For the nonlinear analysis at 10 psi, the axial load carried by the stringer is increased to about 861.4 lbs. However, the axial force in the stringer increases slightly from its minimum value midway between the rings to a maximum at the ring location. The bending moment in the ring is reduced by the geometric nonlinearity at the expense of an increase in value of the circumferential force $N_{\theta r}$ as shown in Fig. 16. The circumferential force in the ring is nearly uniform and increases from 7,242 lbs in the linear analysis to 7,757 lbs in the nonlinear analysis. Thus, the force resultants in the stiffeners increase due to the inclusion of geometric nonlinearity in the analysis.

Singularity at stiffener intersection

The results for the interacting normal loads (Figs. 12 and 14) suggest that they exhibit singular behavior at the stiffener intersection. The argument for singular behavior is supported by plotting the magnitude of the interacting normal load at the stiffener intersection as M and N increase. The total normal load intensity acting on the cylinder at the stiffener intersection is denoted by λ_ζ, where $\lambda_\zeta = \lambda_{\zeta r}(0) + \lambda_{\zeta s}(0)$. This value is -1,190 lb/in from the linear analysis and is reduced to -725 lb/in in the nonlinear analysis for $M = N = 16$. A normalized value of λ_ζ is plotted versus increasing M and N values, with $M = N$, in Fig. 17 for the linear analysis, and in Fig. 18 for the nonlinear analysis. The normalization factor, $\lambda_{\zeta max}$, is simply the value of λ_ζ for the largest values of M and N considered in each analysis. As shown in the figures, λ_ζ is steadily increasing with an increasing number of terms in the truncated Fourier Series. Consequently, the series for λ_ζ does not exhibit, in the range of M and N considered, a convergent behavior. In spite of the fact that the normal load intensity at the stiffener intersection is exhibiting singular behavior, the *total* radial resultant load at the stiffener intersection converges rapidly with increasing values of M and N as shown in Figs. 17 and 18. The total radial resultant plotted in these figures is defined by

$$F_\zeta = \int_{-\Theta}^{\Theta} (\lambda_{\zeta r}\cos\theta - \lambda_{\theta r}\sin\theta)\,(R_0 + e_r)\,d\theta, \tag{36}$$

since the resultant from the stringer vanishes by Eq. (8). From the linear analysis F_ζ = -342.8 lbs, and from the nonlinear analysis F_ζ = -375.5 lbs. Since the applied radial load due to internal pressure acting on the repeating unit is 1,160 lbs (= 10 psi × 20 in × 5.8in), the ring resists about 29.6% of this applied load in the linear response, and this percentage is increased slightly to 32.4% in the nonlinear response. The remaining portion of the applied radial pressure load is carried by the shell.

Conclusions

The spatial distribution of the normal displacements of the cylindrical shell is more uniform, and the bending strains are reduced, in the geometrically nonlinear elastic analysis with respect to what is predicted by the linear elastic analysis. That is, pillowing of the skin is reduced by inclusion of the geometric nonlinearity into the analysis.

The series for the interacting normal load intensity at the stiffener intersection does not appear to converge in both the linear analysis and in the geometrically nonlinear analysis. The magnitude of the resultant normal load intensity at the stiffener intersection using a truncated series approximation is decreased by inclusion of the geometric nonlinearity into the analysis. However, the Fourier Series for the total radial resultant load carried by the stiffeners, which is resolved at the intersection, exhibits rapid convergence. This total radial resultant carried by the stiffeners is increased slightly by the inclusion of the geometric nonlinearity into the analysis. The axial force carried by the stringer due to the closed-end pressure vessel effect is increased in the nonlinear analysis with respect to its value in the linear analysis. Also, the circumferential force carried by the ring is increased in the nonlinear analysis with respect to its value in

the linear analysis. Thus, the stiffeners resist an increased portion of the internal pressure load, accompanied by a commensurate decrease in the load carried by the shell, when geometric nonlinearity is included into the analysis.

Acknowledgment

This research was sponsored by NASA Grant NAG-1-537. Dr. James H. Starnes, Jr., Head, Aircraft Structures Branch, Langley Research Center, is the technical monitor.

References

[1]Sanders, J. L., "Nonlinear Theories for Thin Shells," *Quarterly of Applied Mathematics*, Vol. 21, No. 1, 1963, pp. 21-36.

[2]Sanders, J. L., "An Improved First-Approximation Theory for Thin Shells," NASA Technical Report R-24, June, 1959.

[3]Dong, S. B., Pister, K. S., and Taylor, R. L., "On the Theory of Laminated Anisotropic Shells and Plates," *Journal of the Aerospace Sciences*, Vol. 29, No. 8, August, 1962, pp. 969-975.

[4]Wang, J. T-S, and Hsu, T-H., "Discrete Analysis of Stiffened Composite Cylindrical Shells," *AIAA Journal*, Vol. 23, No. 11, 1985, pp. 1753-1761.

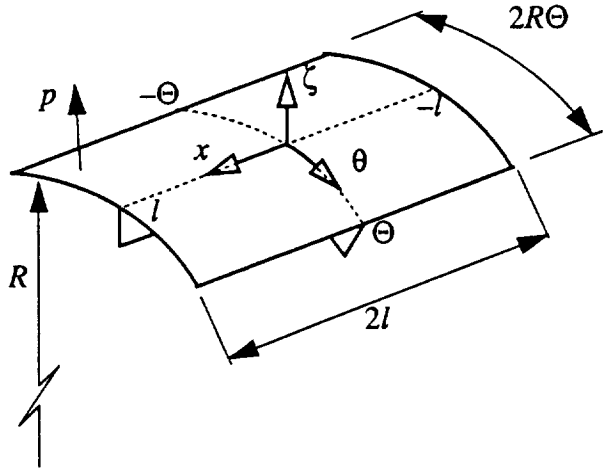

Fig.1 Structural repeating unit of an orthogonally stiffened cylindrical shell subjected to internal pressure p.

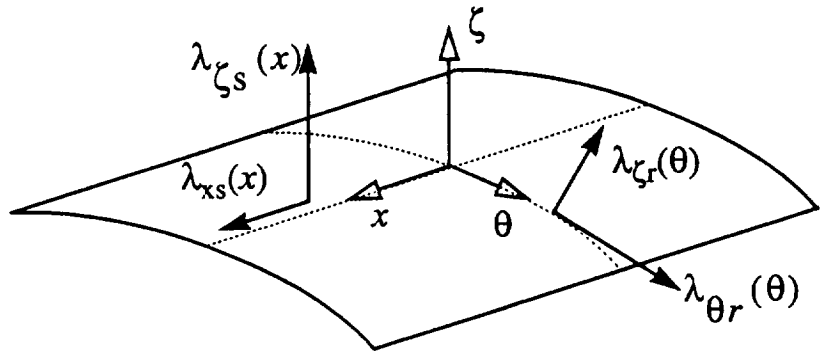

Fig.2 Distributed line load intensities (lb/in) acting on the cylindrical shell due to the ring and stringer.

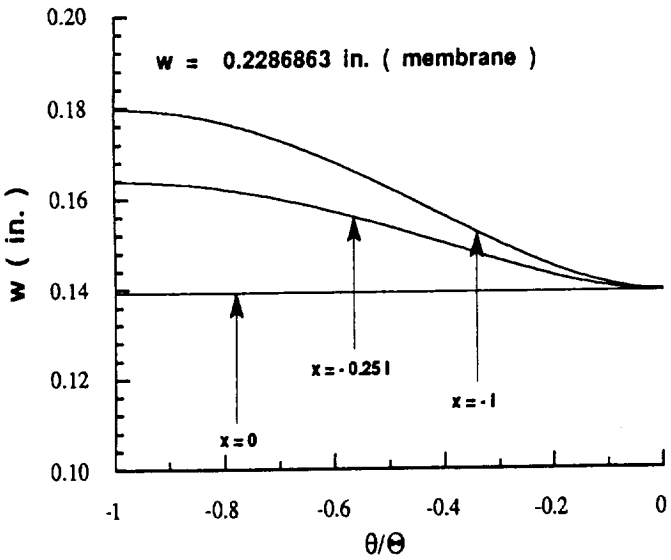

Fig.3 Circumferential distribution of the shell's normal displacement from the linear analysis.

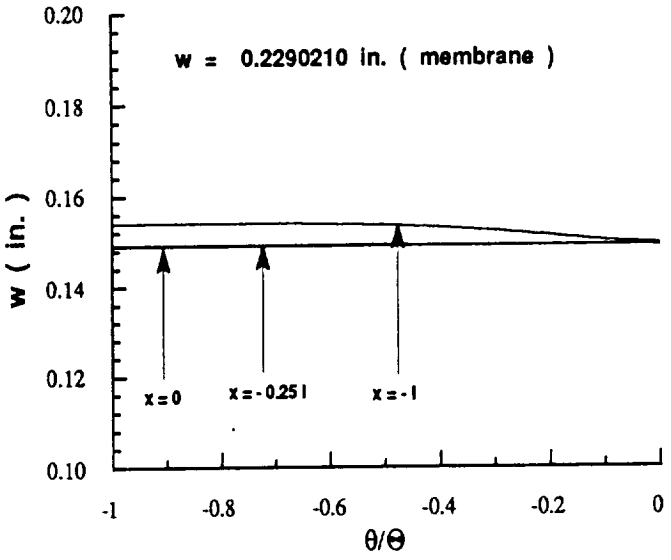

Fig.4 Circumferential distribution of the shell's normal displacement from the nonlinear analysis.

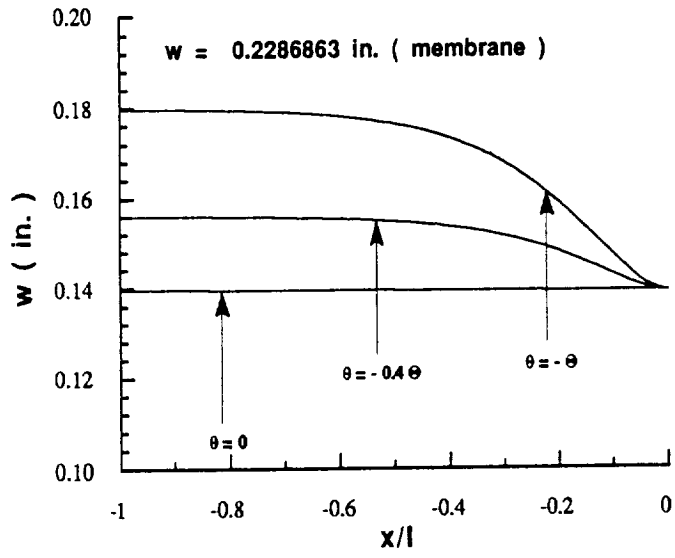

Fig.5 Axial distributions of the shell's normal displacement from the linear analysis.

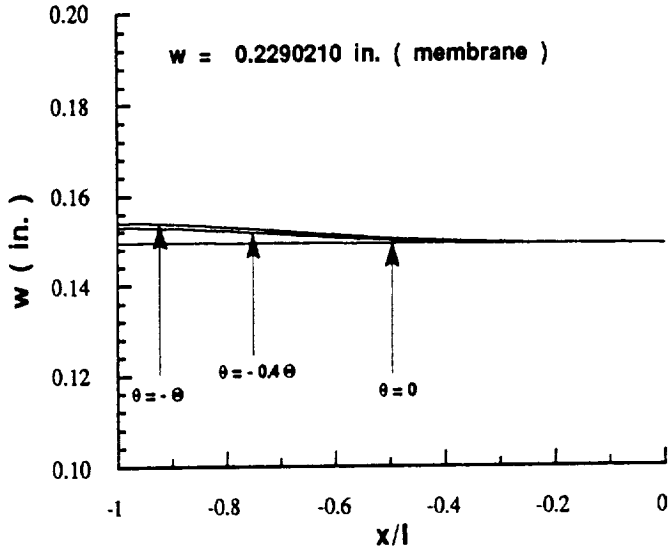

Fig.6 Axial distribution of the shell's normal displacement from the nonlinear analysis.

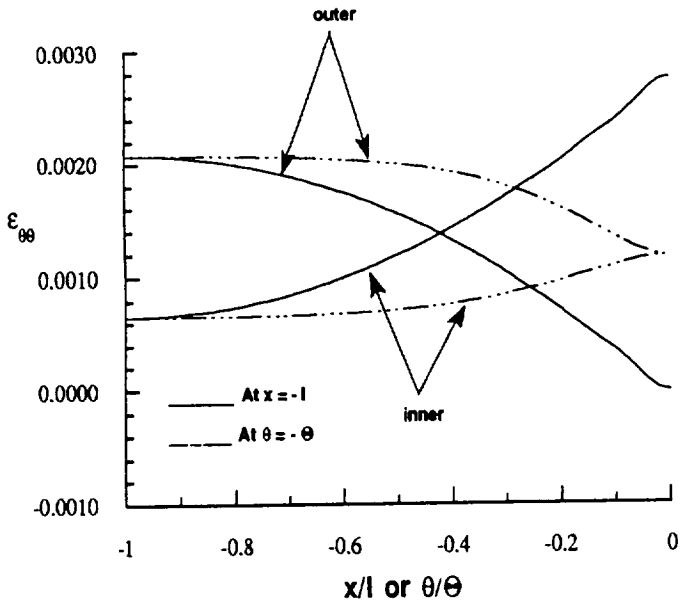

Fig.7 Circumferential normal strain on the inner and outer shell surfaces from the linear analysis.

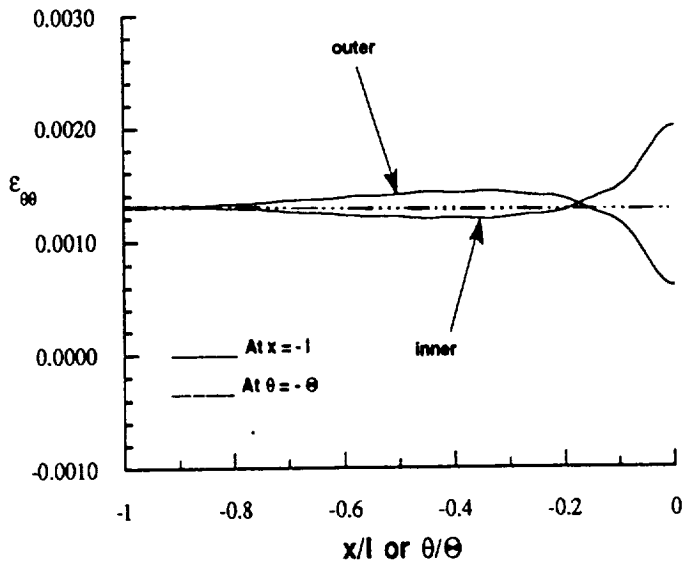

Fig.8 Circumferential normal strain on the inner and outer shell surfaces from the nonlinear analysis.

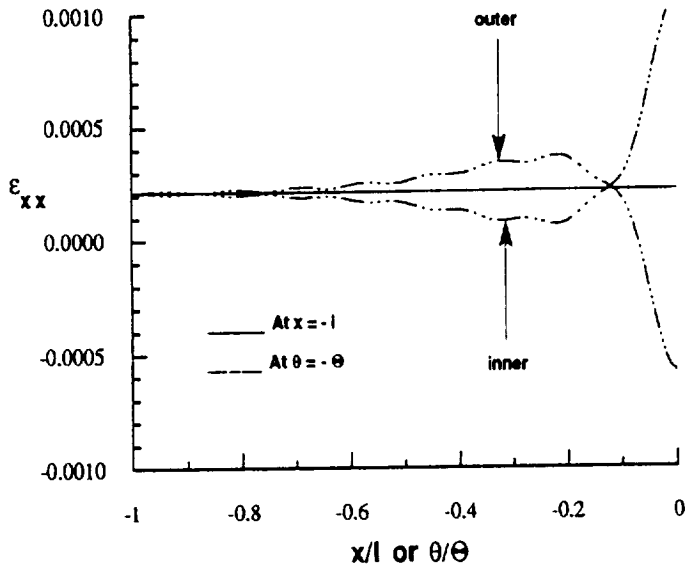

Fig.9 Axial normal strain on the inner and outer shell surfaces from the linear analysis.

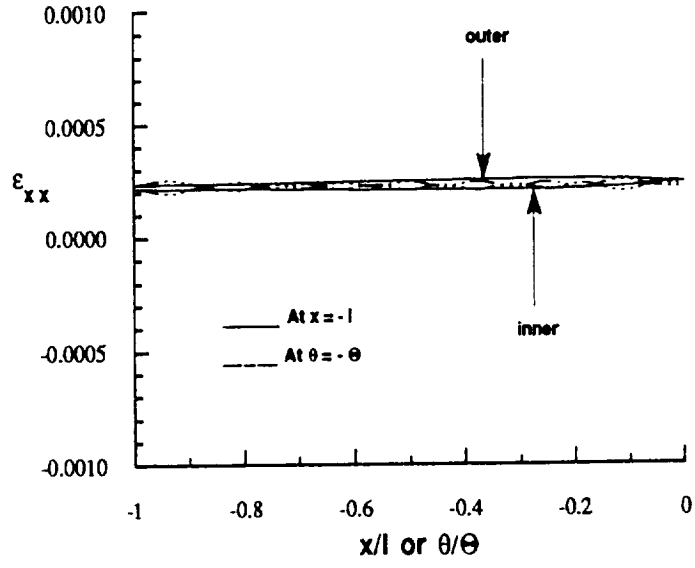

Fig.10 Axial normal strain on the inner and outer shell surfaces from the nonlinear analysis.

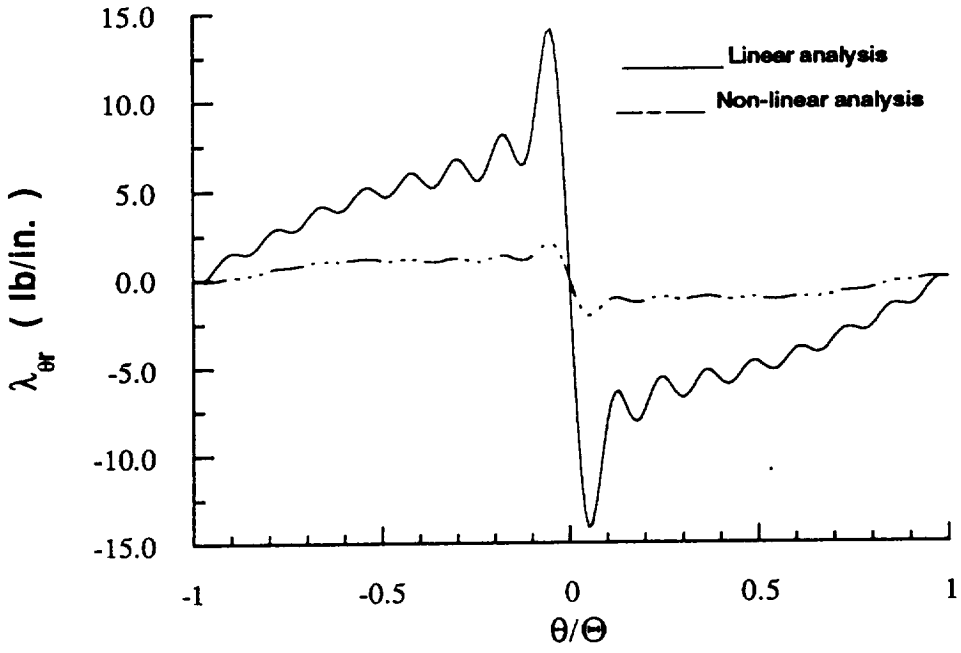

Fig.11 Tangential component of the line load acting on the shell due to the ring.

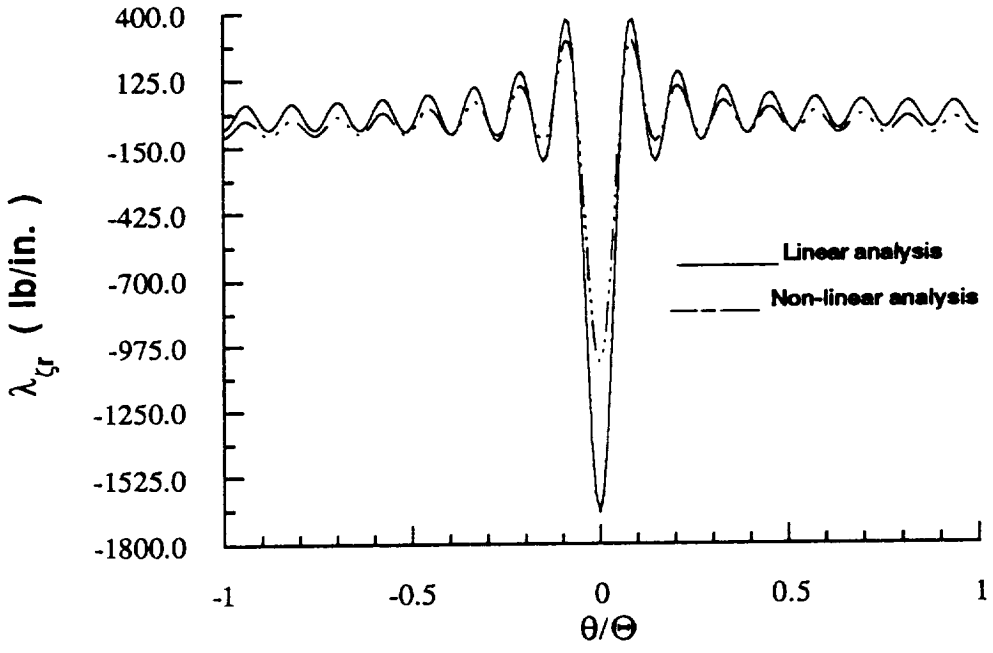

Fig.12 Normal component of the line load acting on the shell due to the ring.

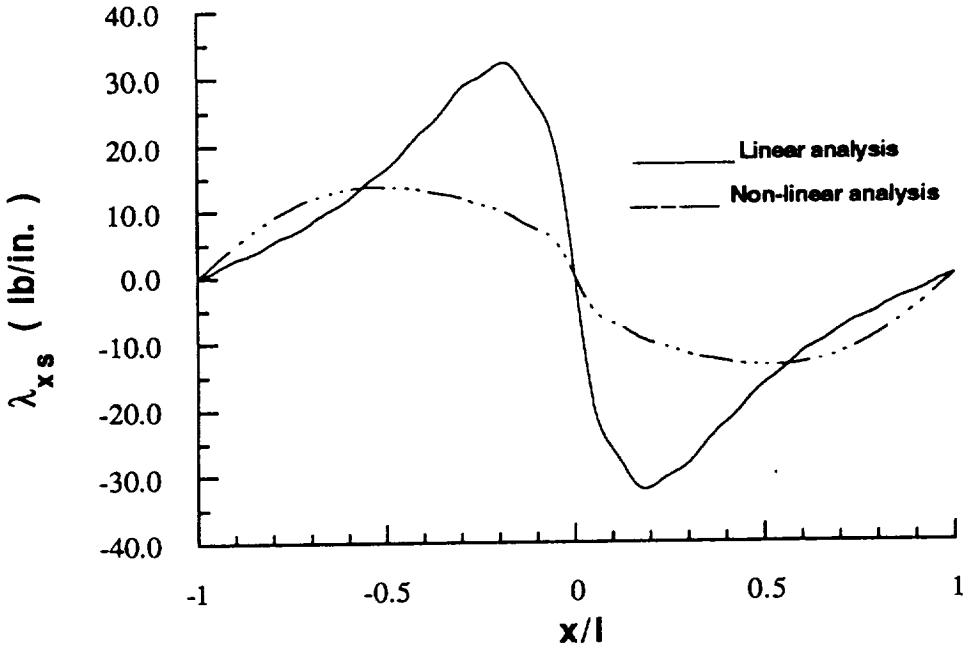

Fig.13 Tangential component of the line load acting on the shell due to the stringer.

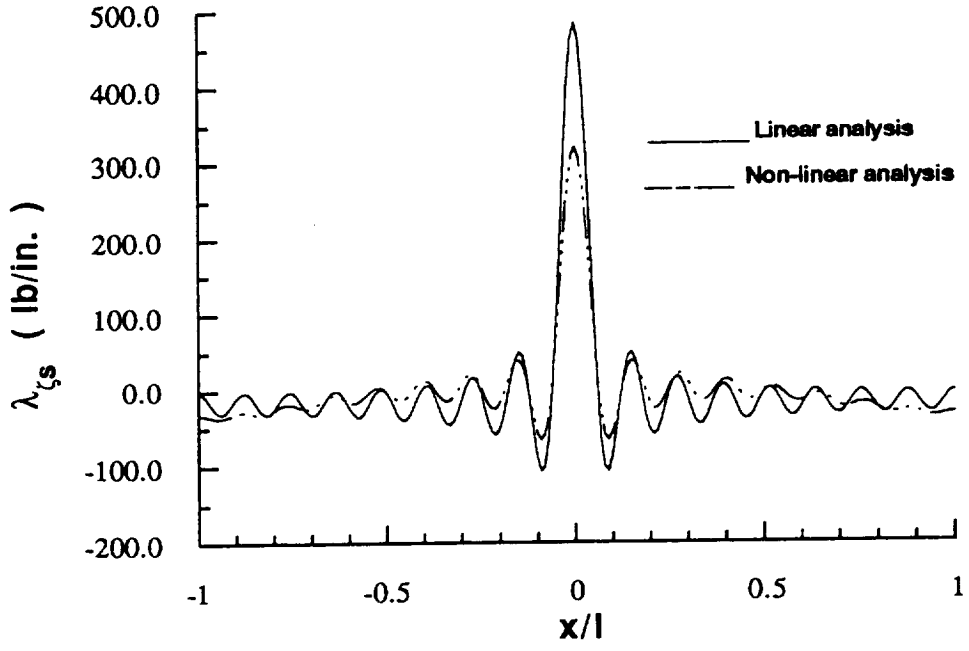

Fig.14 Normal component of the line load acting on the shell due to the stringer.

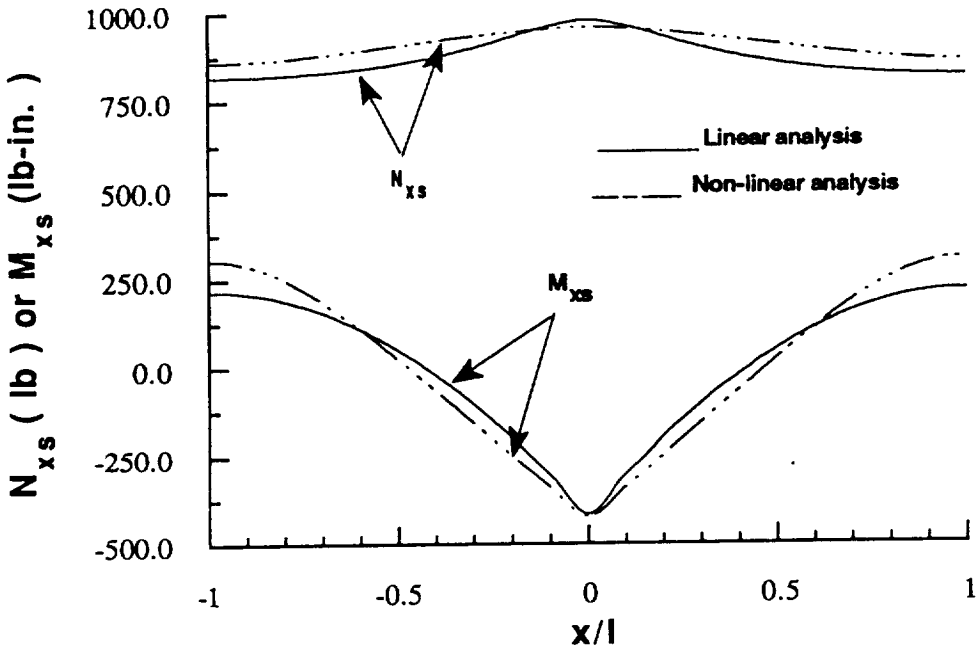

Fig.15 Stringer axial force and bending moment.

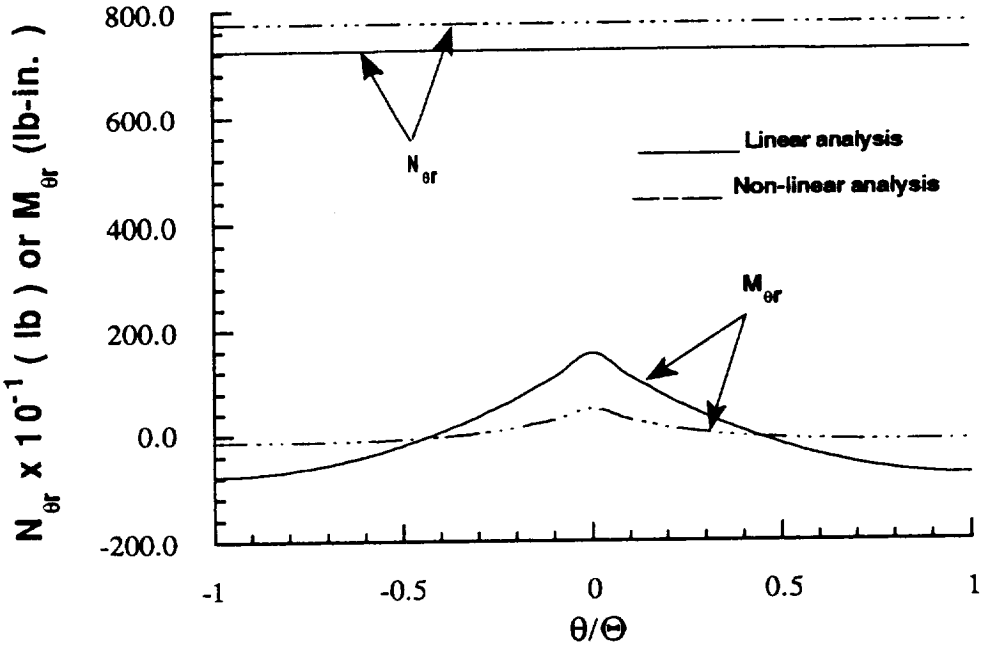

Fig.16 Ring circumferential force and bending moment.

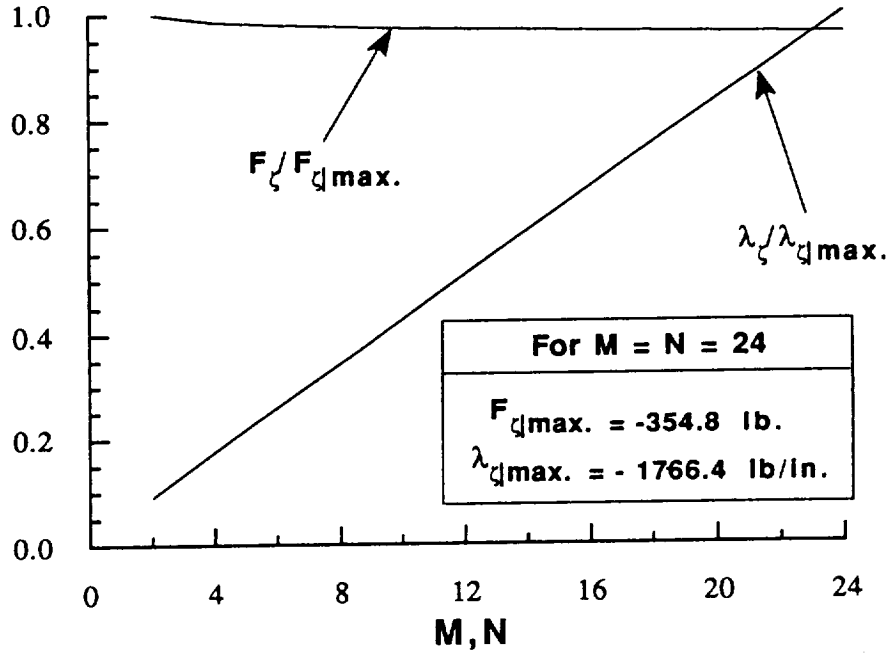

Fig.17 Normal load intensity λ_ζ and total normal load F_ζ at the stiffener intersection for increasing number of harmonics in the linear analysis.

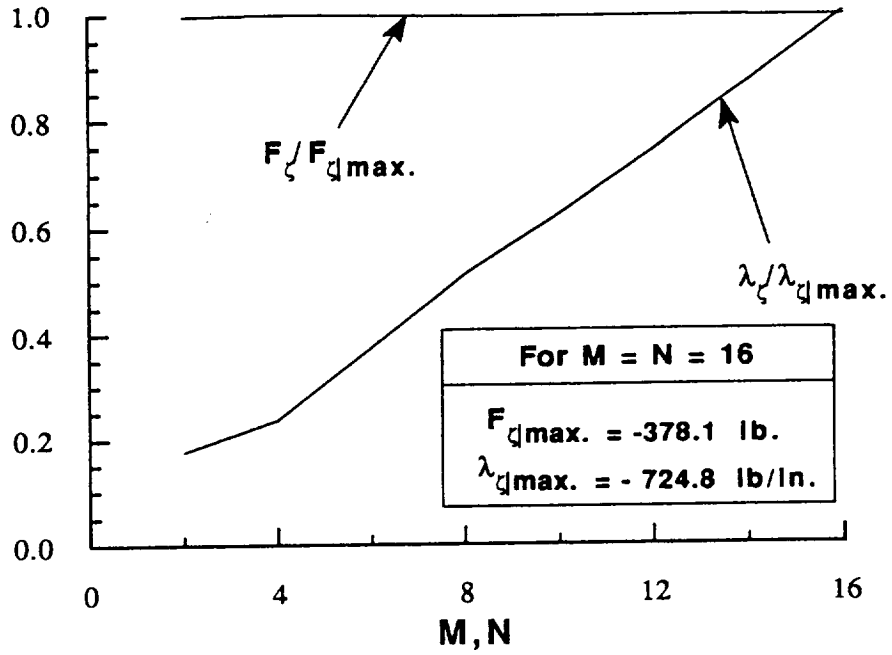

Fig.18 Normal load intensity λ_ζ and total normal load F_ζ at the stiffener intersection for increasing number of harmonics in nonlinear analysis.